JOURNAL OF MATERIALS SCIENCE 25 (1990) 487–492

Dielectric relaxator behaviour of the system $Sr_{1-x}La_xTi_{1-x}Co_xO_3$ ($x \leqslant 0.40$)

OM PARKASH, CH. DURGA PRASAD
School of Materials Science and Technology, Institute of Technology, Banaras Hindu University, Varanasi 221 005, India

DEVENDRA KUMAR
Department of Ceramic Engineering, Institute of Technology, Banaras Hindu University, Varanasi 221 005, India

The dielectric behaviour of the valence-compensated solid solution $Sr_{1-x}La_xTi_{1-x}Co_xO_3$ (x = 0.05, 0.10, 0.20, 0.30 and 0.40) has been studied as a function of temperature and frequency. Compositions with x = 0.20, 0.30 and 0.40 exhibit high values of dielectric constant. This high dielectric constant is due partly to the presence of interfacial polarization, and partly to the formation of grain-boundary barrier layers in these materials. The presence of barrier layers is shown by complex plane impedance analysis.

1. Introduction

Donor-doped strontium titanate, $SrTiO_3$, shows enhanced permittivity on sintering in air [1, 2]. This has been explained on the basis of the formation of barrier layers in such materials. It has been proposed that doping with donor ions facilitates the loss of oxygen from the ceramic during firing according to the reaction

$$O_o \rightleftharpoons \tfrac{1}{2}O_2 + V_o + 2e' \quad (1)$$

where all species are written in accordance with Kroger Vink notation of defects. The presence of donor ions also retards the reoxidation of the ceramic during cooling from firing temperature to room temperature. Because of insufficient time available during cooling, reoxidation is restricted to the grain boundaries only, making them insulating. The grains still remain semiconducting. This gives rise to barrier layers at grain–grain-boundary interfaces, imparting very high permittivity to the resulting products [1]. Semiconducting $SrTiO_3$ is also obtained by heating in atmospheres of low partial pressure of oxygen [3]. The resistance of the grain boundaries can be increased by impregnating them with insulating oxides. This is used as a basis for the manufacture of boundary layer capacitors [4, 5].

We synthesized various compositions in the system $Sr_{1-x}La_xTi_{1-x}Co_xO_3$ to study the possibility of formation of the solid solution between $SrTiO_3$ and $LaCoO_3$ [6, 7] and to investigate the electrical behaviour of the resulting samples. Single phase materials are obtained for all values of x in this system, indicating the formation of the solid solution over the entire composition range. In this system, simultaneous substitution of La^{3+} for Sr^{2+} and Co^{3+} for Ti^{4+} maintains the electrical charge neutrality internally. Such a solution is termed as a valence-compensated solid solution. The electrical behaviour and the spin and valence-state equilibria of the cobalt ions, using Mossabauer spectroscopy, have been reported earlier [8] for compositions with $x \geqslant 0.50$. In this paper we are reporting the dielectric behaviour of the materials with $x \leqslant 0.40$. This forms the first report on the dielectric behaviour of these materials, to the best of our knowledge.

2. Experimental procedure

All the samples were prepared by the ceramic method using strontium oxalate, lanthanum oxalate, cobalt oxalate and titanium dioxide, all having better than 99.5% purity. The details of the method of preparation have been reported earlier [6]. Powder X-ray diffraction patterns of the final products were taken using Cu$K\alpha_1$ radiation in a diffractometer (Rigaku Rotaflex). The bulk density of the samples was determined from the mass and geometrical dimensions of the sintered pellets. Percentage porosity was calculated from the values of true density and bulk density of various samples. For dielectric measurements, air-drying silver paint was applied on both surfaces of polished cylindrical pellets. Capacitance and dielectric loss were measured in the frequency range 1 KHz to 1 MHz, at different steady temperatures employing an impedance analyser (Hewlett Packard 4192A LF). The temperature was held constant within $\pm 0.5°C$ during the measurements. Measurements were repeated on at least two pellets of the same composition. Samples with x = 0.20, 0.30 and 0.40 were polished and etched using 5% HNO_3 + 2 to 3 drops of 40% HF. The etched surfaces were coated with gold–palladium alloy and observed in a scanning electron microscope (Philips PSEM-500). For the compositions with x = 0.05 and 0.10, the microstructures of the fractured surfaces of the sintered pellets coated with gold–palladium alloy were observed. This is because of the very fine grain size of these two compositions.

0022–2461/90 $03.00 + .12 © *1990 Chapman and Hall Ltd.*

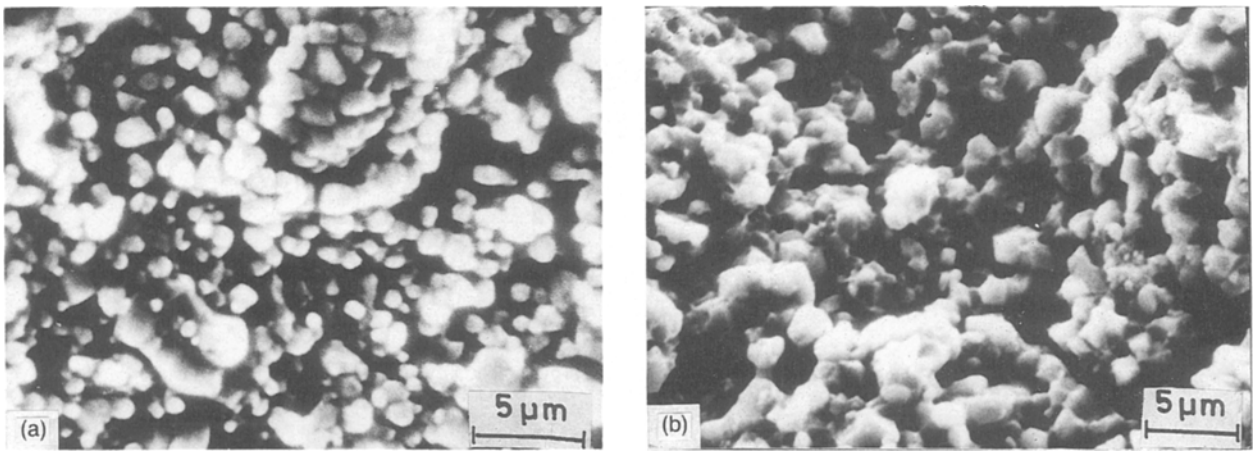

Figure 1 Scanning electron micrographs of the fractured surfaces of samples with (a) $x = 0.05$ (b) $x = 0.10$.

3. Results and discussion

X-ray diffraction data indicated the formation of single-phase materials in all the compositions [6]. The structure remains cubic, similar to $SrTiO_3$, in all the compositions studied (that is for $x \leqslant 0.40$). Lattice parameters of the various compositions as reported earlier [6] are given in Table I. The bulk density and percentage porosity for various compositions are also given in Table I. All the samples except that with $x = 0.40$ had a bulk density greater than 90% of the theoretical density. The composition with $x = 0.40$ had a density 86% of the theoretical value. Typical scanning electron micrographs are shown in Figs 1 and 2. The average grain size of these samples is given in Table I. It is noted from the table that the average grain size is small in these materials.

Variation of the dielectric constant, ε, and dielectric loss, D, for compositions with $x = 0.05$, 0.10, 0.20, 0.30 and 0.40, at 1, 10 and 100 KHz, is shown as a function of temperature in Figs 3 to 7, respectively. The behaviour of the composition with $x = 0.05$ and 0.10 is similar. Two anomalies in the ε against T plots are seen for these two samples. The peak value of ε in the high temperature anomaly decreases with increasing frequency. Its position is almost independent of frequency in both the samples. This is attributed to the process occurring at sample electrode interface, that is, electrode polarization. Similar results have been reported earlier for single crystals of pure $SrTiO_3$ [9]. In the case of pure $SrTiO_3$, this peak occurs at ~ 1000 K. We observe this at much lower temperatures; this may be because of changes in composition in our samples. No such anomaly is seen in the samples with $x \geqslant 0.20$.

The low-temperature anomaly becomes increasingly pronounced with increasing x. Samples with $x = 0.20$, 0.30 and 0.40 exhibit rounded peaks in their ε against T plots whose position shifts to higher temperatures with increasing frequency. The temperature where ε peaks at a particular frequency is higher than the temperature where D peaks. In the sample with $x = 0.20$, the anomaly in the D against T plot at 1 KHz appears at ~ 360 K. The peaks at higher frequencies are not observed distinctly, for reasons discussed later. In the samples with $x = 0.30$, and 0.40, anomalies in the D against T plots are seen above room temperature only at 100 KHz. For lower frequencies (1 and 10 KHz) these seem to occur below 300 K. Both ε and D show strong frequency dependence, which becomes more pronounced near the peak temperatures. All these features show that these compositions exhibit dielectric relaxator behaviour. Values of ε and D at 1 KHz and 300 K for all the samples are given in Table II.

Plots of ε and D against $\log f$ at a few temperatures for the composition with $x = 0.30$ are shown in Fig. 8. Similar behaviour is observed for the sample with $x = 0.40$. Strong dispersion is observed in the value of ε in the frequency range 1 KHz to 1 MHz, the dispersion increasing with increasing temperature. D against $\log f$ plots show peaks at a particular frequency which increases with increasing temperature. Both these features support the idea that these materials are relaxators. The relaxational polarization arises due to the presence of microheterogeneities in these materials which are present due to the slow thermochemical diffusion-controlled ceramic processing used for their preparation. The presence of these microregions with different conductivities (because of different compositions) gives rise to interfacial or space-charge

TABLE I Lattice parameter, a(nm), bulk density ($g\,cc^{-1}$), percentage porosity, average grain size, dielectric constant (ε) and dielectric loss (D) at 1 KHz and 300 K for various samples in the system $Sr_{1-x}La_xTi_{1-x}Co_xO_3$

x	a(nm)	Bulk density ($g\,cc^{-1}$)	Porosity (%)	Average grain size (μm)	ε	D
0.05	0.3898	5.22	5.00	1–2	1370	0.80
0.10	0.3875	5.31	7.00	1–2	540	1.12
0.20	0.3880	5.50	8.00	2–3	410	0.95
0.30	0.3870	5.74	8.00	2–3	43800	1.14
0.40	0.3865	5.99	14.00	2–3	18670	5.60

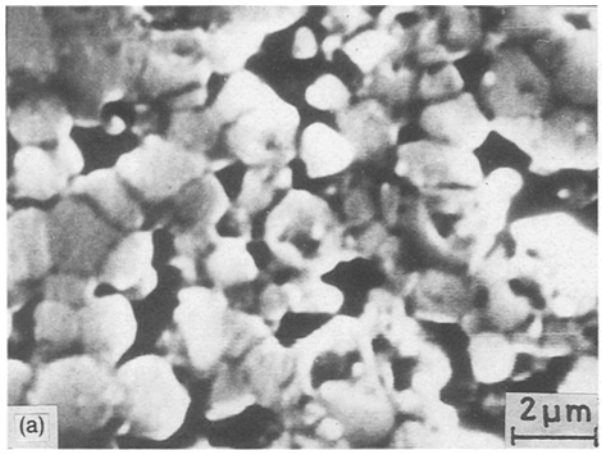

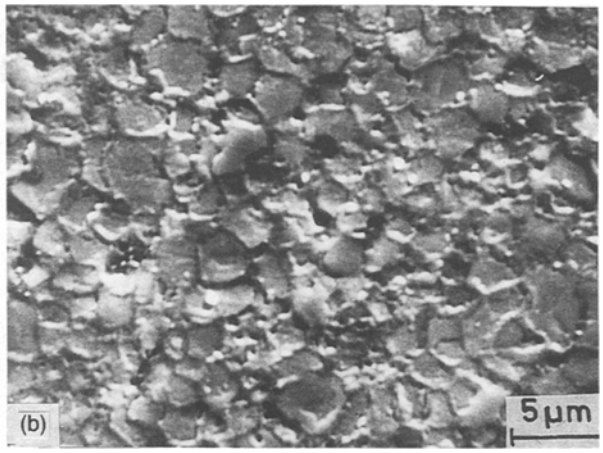

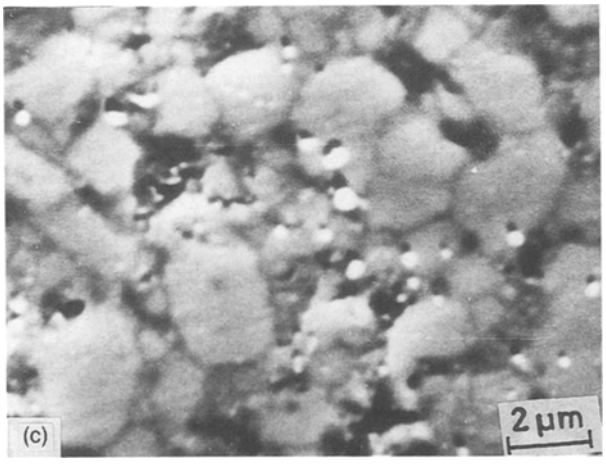

Figure 2 Scanning electron micrographs of chemically etched samples with (a) $x = 0.20$; (b) $x = 0.30$; (c) $x = 0.40$.

polarization. The interfacial polarization cannot follow the rapidly changing field leading to the observed dispersion in ε.

The variation of ε with temperature obeys the relation [10]

$$\frac{1}{\varepsilon} = \frac{1}{\varepsilon_{max}} + \frac{(T - T_c)^2}{c_2} \qquad (2)$$

both above and below the temperature where ε_{max} peaks at a given frequency and c_2 is a constant for a given frequency. The plots of $(\varepsilon - \varepsilon_{max})^{-1}$ against $(T - T_c)^2$ above T_c at 1 KHz for the compositions with $x = 0.20$, 0.30 and 0.40 are shown in Fig. 9. These plots are linear over a range of temperatures both above and below T_c. This relation is obeyed at other frequencies also. The temperature regions where Equation 2 is obeyed at various frequencies in the compositions with $x = 0.20$, 0.30 and 0.40 are given in Table II. We have not plotted these curves for the compositions with $x = 0.05$, and 0.10, because both ε_{max} and T_c are not well defined in these two samples for the low temperature peaks in their ε against T plots (Figs 2 and 3).

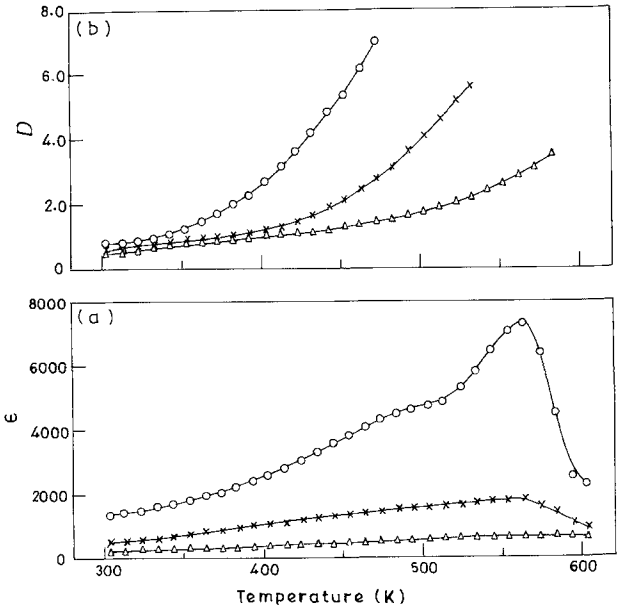

Figure 3 Variation of (a) ε and (b) D with temperature for the sample with $x = 0.05$ in the system $Sr_{1-x}La_xTi_{1-x}Co_xO_3$. ○, 1 KHz; ×, 10 KHz; △, 100 KHz.

Equation 2 is applicable in those materials which have contributions both from an interfacial polarization and a ferroelectric polarization. Our samples have interfacial polarization, as discussed above. Although the overall symmetry of these samples is cubic, there may be local deviations from the cubic symmetry in these materials because of heterovalent substitutions. These local regions will have spontaneous polarization associated with these distortions. Thus we may have local ferroelectric regions weakly connected by non-ferroelectric regions. Such a microstructure gives rise to relaxator behaviour with a high dielectric constant [11].

The high values of dielectric constant in these compositions also seem to be partly due to the barrier layers produced at the grain boundaries during the processing of these materials. This is confirmed by the complex plane impedance analysis. The charge transport through polycrystalline materials involves three processes: (i) bulk conduction or interagranular

TABLE II Temperature range where Equation 2 is obeyed at different frequencies for various samples in the system $Sr_{1-x}La_xTi_{1-x}Co_xO_3$

x	Temperature range (K)		
	1 KHz	10 KHz	100 KHz
0.20	425–525	445–555	485–575
0.30	425–535	500–600	525–600
0.40	315–445	365–475	435–545

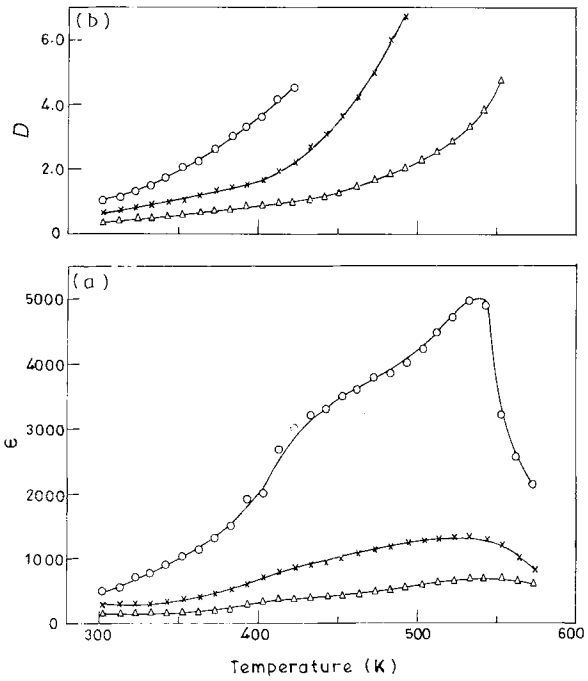

Figure 4 Variation of (a) ε and (b) D with temperature for the sample with $x = 0.10$ in the system $Sr_{1-x}La_xTi_{1-x}Co_xO_3$. ○, 1 KHz; ×, 10 KHz; △, 100 KHz.

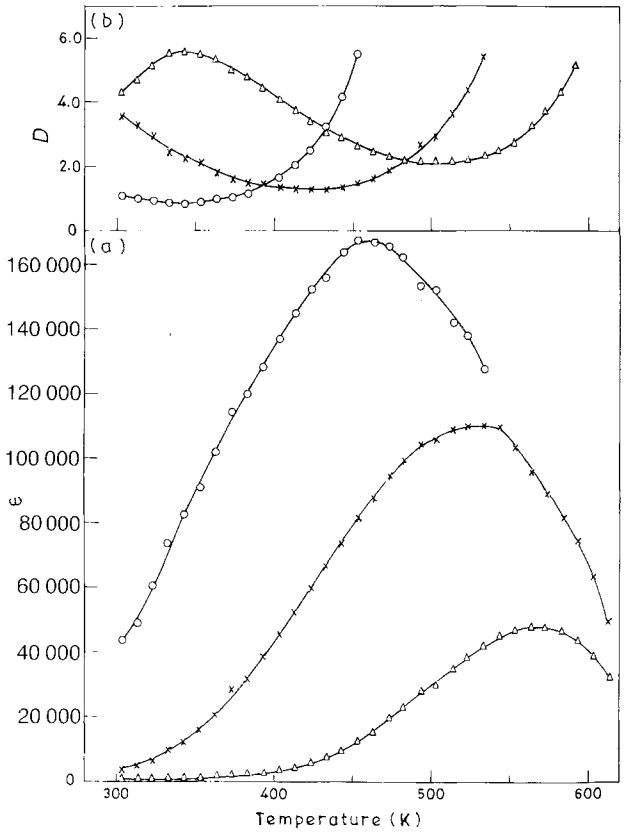

Figure 6 Variation of (a) ε and (b) D with temperature for the sample with $x = 0.30$ in the system $Sr_{1-x}La_xTi_{1-x}Co_xO_3$. ○, 1 KHz; ×, 10 KHz; △, 100 KHz.

conduction; (ii) conduction across the grain boundaries; and (iii) transport across the electrode–specimen interface or electrode polarization. Each process can be represented by an independent equivalent circuit of R and C in parallel. The overall sample then corresponds to three R–C parallel combinations connected in series as shown in Fig. 9. The impedance of an R–C parallel combination is given by

$$Z^* = Z' - iZ'' \tag{3}$$

where Z' and Z'' are the real and imaginary components of total complex impedance, Z^*. In complex plane impedance analysis, the real part of the impedance, Z', is plotted against the imaginary part, Z'', over a range of frequencies. Depending on the relative values of the relaxation times of the three processes mentioned above, we may observe three semi-circular arcs in the impedance plots as given in Fig. 9. Generally, the highest frequency arc represents the bulk conduction, the intermediate arc, the grain boundary conduction, and the lowest arc, the contribution of electrode processes to the total observed

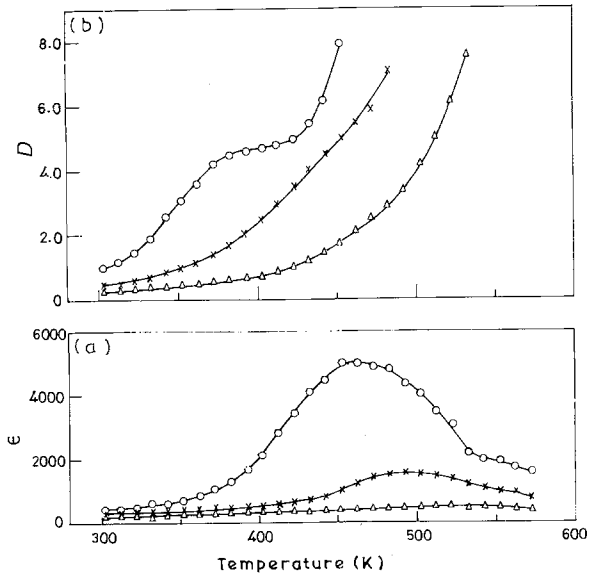

Figure 5 Variation of (a) ε and (b) D with temperature for the sample with $x = 0.20$ in the system $Sr_{1-x}La_xTi_{1-x}Co_xO_3$. ○, 1 KHz; ×, 10 KHz; △, 100 KHz.

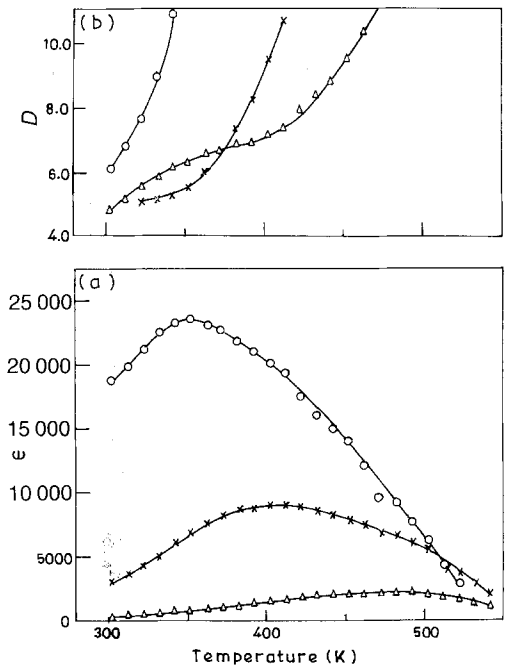

Figure 7 Variation of (a) ε and (b) D with temperature for the sample with $x = 0.40$ in the system $Sr_{1-x}La_xTi_{1-x}Co_xO_3$. ○, 1 KHz; ×, 10 KHz; △, 100 KHz.

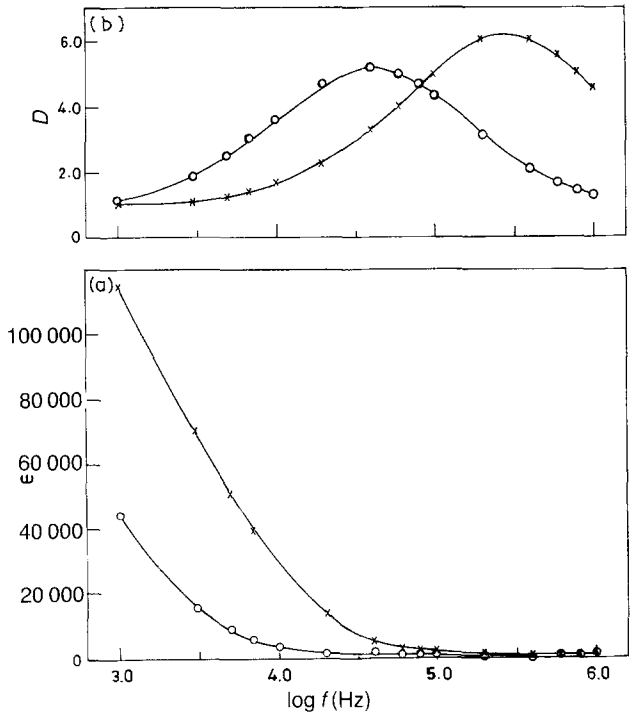

Figure 8 Plots of (a) ε and (b) D against log frequency at temperatures ○, 303 K; ×, 373 K for the sample with $x = 0.30$ in the system $Sr_{1-x}La_xTi_{1-x}Co_xO_3$.

conduction. The resistance values of the three contributions are obtained from the intercept of the circular arcs with the real axis, while the capacitance values are obtained from the highest point in the arc, where

$$\omega RC = 1 \qquad (4)$$

$\omega = 2\pi f$ is the angular frequency at the highest point. Details of impedance analysis are available in the literature [12–15].

Some typical impedance plots of the compositions with $x = 0.30$ and 0.40 are shown in Fig. 10. Two circular arcs with the centre below the Z' axis are

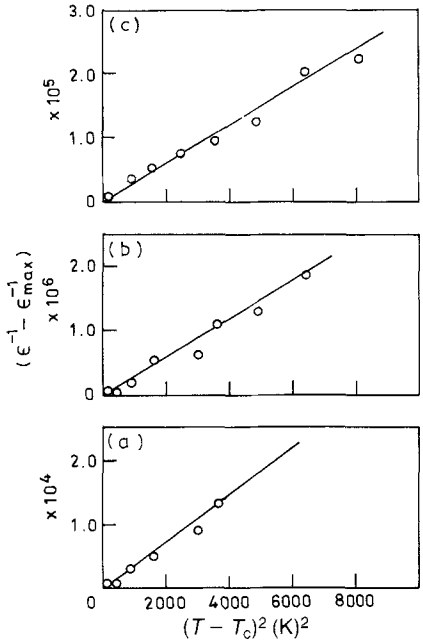

Figure 9 Plots of $(\varepsilon - \varepsilon)^{-1}$ against $(T - T_c)^2$ for the samples with (a) $x = 0.20$, (b) $x = 0.30$ and (c) $x = 0.40$ in the system $Sr_{1-x}La_xTi_{1-x}Co_xO_3$.

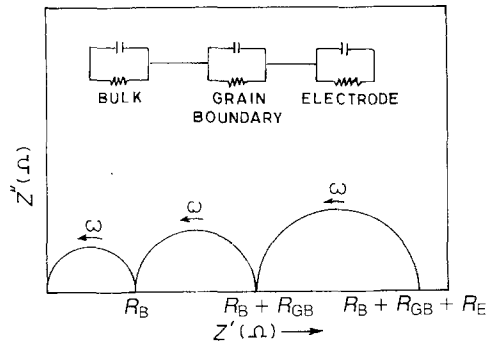

Figure 10 Schematic representation of equivalent circuit and corresponding impedance plot for electrical transport through a polycrystalline material.

observed. The one with higher frequency passing through the origin represents the bulk resistance due to grains, while that in the low frequency range corresponds to the grain-boundary contribution to the total observed resistance. There is no significant contribution from the electrode process as the d.c conductivity of these samples was found to be independent of time, indicating the absence of any electrode polarization [7]. For the sample with $x = 0.40$ at 303 K, the contributions interagranular and intergrain resistance to the total observed resistance are 4.6×10^3 and 4.5×10^3 ohms, respectively. The average grain size of this sample is 2.0 μm. If we assume grain boundaries to be 10 nm or 0.01 μm thick, the ratio of resistivity of the grain boundaries to the grain would be $[(2/0.01) \times (4.5 \times 10^3)/(4.6 \times 10^3) = 195]$.

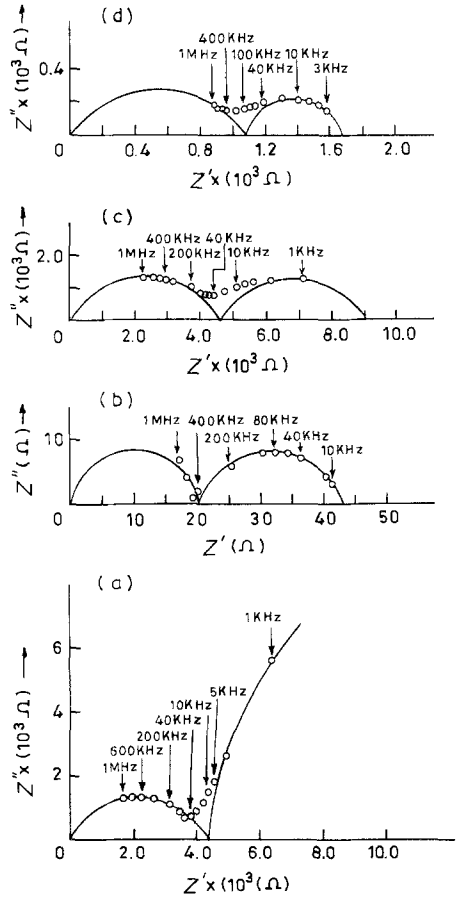

Figure 11 Typical impedance plots of the system $Sr_{1-x}La_xTi_{1-x}Co_xO_3$. (a) $x = 0.30$, $T = 303$ K; (b) $x = 0.30$, $T = 573$ K; (c) $x = 0.40$, $T = 303$ K; (d) $x = 0.40$, $T = 373$ K.

Hence the grain boundaries are more resistive as compared to the bulk of the sample. This confirms the formation of barrier layers in these materials. The formation of barrier layers is further confirmed by measuring the dielectric constant on the same pellet after removing silver paint and coating it with gold–palladium alloy. This eliminates any variation of ε due to change in the dimensions and microstructure of the sample. The values observed for the composition with $x = 0.30$ are 36400, 1390 and 320, while the values observed with silver paint are 43800, 3470 and 350 at 1, 10 and 100 KHz, respectively. This also supports the formation of barrier layers in these materials as their dielectric constant depends on the method of electrode application [2].

The mechanism of barrier layer formation is similar to that in donor-doped $SrTiO_3$ as mentioned in the introduction. The presence of cobalt at the titanium site in $BaTiO_3$ and $SrTiO_3$ produces oxygen deficiency to maintain the electrical charge neutrality [11]. Therefore, the simultaneous presence of lanthanum and cobalt will promote the loss of more oxygen during the firing process as compared to only lanthanum-doped $SrTiO_3$.

The dielectric loss in these materials increases with x, that is, with increasing cobalt concentration. This is largely due to the increase of d.c. conductivity with cobalt concentration whose **3d** electrons are mainly responsible for conduction in these materials. All other ions have a closed shell configuration of inert gases, and are not expected to participate in the conduction.

We are currently synthesizing these materials in different atmospheres; results of these investigations will be published shortly.

Acknowledgements

Financial support from the Department of Science and Technology, Government of India, New Delhi is gratefully acknowledged.

References

1. G. I. SKANAVI and E. M. MATVEENA, *Soviet. Phys.* **3** (1957) 905.
2. I. BURN and S. NEIRMAN, *J. Mater. Sci.* **17** (1982) 3510.
3. S. WAKU, *Rev. Elect. Commun. Lab.* **15** (1967) 689.
4. R. M. GLAISTER and J. W. WOOLNER, *J. Elect. Control* **6** (1959) 385.
5. N. YAMAOKA, *Bull. Amer. Ceram. Soc.* **65** (1986) 1149.
6. O. PARKASH, CH. D. PRASAD and D. KUMAR, *Phys. Stat. Solidi a* in press.
7. *Idem, J. Solid State Chem.* in press.
8. V. KUMAR, *et al. Phys. Stat. Solidi b* **128** (1985) 223.
9. R. STUMPH, D. WAGNER and D. BAUERLE, *ibid. a* **75** (1983) 143.
10. V. V. KIRILLOV and V. A. ISUPOV, *Ferroelectrics* **5** (1973) 3.
11. R. E. NEWNHAM, *J. Mater. Educ.* **5** (1983) 941.
12. J. E. BAUERLE, *J. Phys. Chem. Solids* **30** (1969) 2657.
13. J. R. MACDONALD, *J. Chem. Phys.* **61** (1974) 3977.
14. *Idem.* "Superionic Conductors", edited by G. D. Mahan and W. L. Roth (Plenum, New York, 1976) p. 81.
15. A. D. FRANKLYN, *J. Amer. Ceram. Soc.* **58** (1975) 465.

Received 28 September 1988
and accepted 13 April 1989